Journal of ELECTRONIC MATERIALS, Vol. 46, No. 7, 2017
DOI: 10.1007/s11664-017-5324-0

Impedance Spectroscopy Analysis of $Mg_4Nb_2O_9$ Ceramics with Different Additions of V_2O_5 for Microwave and Radio Frequency Applications

J.M.S. FILHO,[1,2,5] C.A. RODRIGUES JUNIOR,[4] D.G. SOUSA,[3] R.G.M. OLIVEIRA,[1] M.M. COSTA,[3] G.C. BARROSO,[4] and A.S.B. SOMBRA[2]

1.—Department of Teleinformatics Engineering, Technology Center, Federal University of Ceará, Fortaleza, Ceará 60755-640, Brazil. 2.—Department of Physics, Laboratory of Telecommunications and Science and Materials Engineering (LOCEM), Federal University of Ceará, P.O. Box 6030, Fortaleza, Ceará 60455-760, Brazil. 3.—Institute of Physics, LACANM, UFMT, Cuiabá, MT 78060-900, Brazil. 4.—Department of Electrical Engineering, Federal University of Ceará (UFC), Fortaleza, Ceará, Brazil. 5.—e-mail: jmsfilho@sfiec.org.br

The complex impedance spectroscopy study of magnesium niobate $Mg_4Nb_2O_9$ (MN) ceramics with different additions of V_2O_5 (0%, 2%, 5%) was performed in this present paper. The preparation of MN samples were carried out by using the solid-state reaction method with a high-energy milling machine. Frequency and temperature dependence of the complex impedance, complex modulus analysis, and conductivity were measured and calculated at different temperatures by using a network impedance analyzer. A non-Debye type relaxation was observed showing a decentralization of the semicircles. Cole–Cole formalism was adopted here with the help of a computer program used to fit the experimental data. A typical universal dielectric response in the frequency-dependent conductivity at different temperatures was found. The frequency dependent ac conductivity at different temperatures indicates that the conduction process is thermally activated. The activation energy was obtained from the Arrhenius fitting by using conductivity and electrical modules data. The results would help to understand deeply the relaxation process in these types of materials.

Key words: Complex impedance spectroscopy, dielectric microwave materials, Cole–Cole formalism

INTRODUCTION

Microwave and radio frequency devices based on dielectric materials have strongly increased the demand for materials, which can meet all the specifications required for communication systems, such as a high quality factor (Q_f), an appropriate dielectric constant (ε_R), and a near-zero temperature coefficient of resonant frequency (τ_f). Besides these essential and applicable parameters for communication applications, there is also a concern of optimizing the process of production of these materials for a more facility to guarantee a coming perspective of manufacturing telecommunication devices, for example, sintering temperature, heating/cooling rate, milling time, dwell time in furnace were also taken into account in this present paper. The corundum-like phase of magnesium niobate MN with a high Q_f, is a suitable material for microwave applications specially because of its dielectric constant and high quality factor values which are comparable to those of sintered Al_2O_3.[1,2] It is also an important material, which shows self-activated photoluminescence at room temperature.[3,4] The method to produce MN powders of precise stoichiometry and desired properties depending on a number of variables such as raw

(Received September 10, 2016; accepted January 18, 2017; published online March 6, 2017)

materials, their purities, processing history, temperature, time, and so on.[5,6] In general, production of single-phase MN ceramic is not straightforward, as minor concentrations of the $MgNb_2O_6$ phases and/or MgO inclusion are sometimes formed alongside the major phase of $Mg_4Nb_2O_9$.[7] The preparation of MN samples to be investigated was accomplished by using the solid-state reaction technique consisting of a simple and non-incisive process, which differs from other methods involving preparation of chemistry solutions.[8,9] The choice of V_2O_5 to be added to MN ceramics was for lowering the sintering temperature without worsening the dielectric and microwave properties. In this present paper, a previously series of samples with different percentages (0%, 2%, 5%) of V_2O_5 additions has been prepared in order to investigate the effect on MN ceramics. Better results were found in favor of the MN02 specimen, which is presented here. Impedance parameters were measured by a Solartron 1260A Impedance/Gain-phase Analyzer™. The pellets were fabricated appropriately contained in a cylindrical thermal chamber where the temperature was kept constant and stable while varying the frequency from 1 Hz to 1 MHz at various temperatures (305–430°C). The impedance measurements of the specimens to be visualized and analyzed were collected by a network computer program.

EXPERIMENTAL PROCEDURES

Material Preparation

The starting powdered materials used in this present paper were commercially available magnesium oxide, MgO (99.9% purity) and niobium oxide, Nb_2O_5 (99.5% purity) for formation of single-phase $Mg_4Nb_2O_9$ ceramic. Both MgO and Nb_2O_5 powders were individually weighed for the following stoichiometric formula: $4MgO + Nb_2O_5$. They also were individually heated in a conventional oven at 150°C for 2 h in order to eliminate excess water absorbed from the air. Preheated oxides were mixed thoroughly in an agate mortar and put them in an alumina crucible for the calcination process by using a programmable furnace with heating/cooling rate of 5°C/min and a 5-h dwell time at 1000°C. The formation of the compound was confirmed by x-ray diffraction (XRD) and no other second phase was detected. The XRD pattern of the calcined powders was found using an XRD powder diffractometer with CoKα radiation ($\lambda = 1.788965$ Å) in a wide range of Bragg angles 2θ ($20° < 2\theta < 80°$) at a scanning rate of 0.5°/min. The fine and homogeneous calcined pure powders were used to prepare a series of three specimens with different additions of V_2O_5 (0%:MN00, 2%:MN02, and 5%:MN05). Then, the specimens were pressed into circular pellets of ~15 mm diameter and thickness ~1–2 mm by applying a pressure of 6 MPa using an axial hydraulic press. Polyvinyl alcohol (PVA) was used as the binder to reduce the brittleness of the pellets. The organic binder was burnt out during sintering process. The sintering process was carried at 1100°C for 6 h. The sintered pellets were polished on fine emery paper in order to make both the faces flat and parallel. The polished faces were then electroded with high purity silver paste. The frequency and temperature dependent dielectric measurements were carried out using an Agilent 4294A (40 Hz–110 MHz) Solartron SI 1260 (0.1 Hz–32 MHz)impedance analyzer appropriately connected to a network computer and using a programmable electrometer and heating arrangements. For this purpose, pellets were kept at 100°C for 14 h before taking any measurement in order to avoid rehydration during experiments. All the measurements were carried out in dry air.

RESULTS AND DISCUSSION

Structural Properties

In order to identify the one-phase material, XRD analysis was carried out, the sample data were identified, and the powder diffraction pattern of $Mg_4Nb_2O_9$ ceramics was plotted as the measured intensity. These patterns agree with inorganic crystal structure database (ICSD) data as shown in Fig. 1.

The refinement was carried out by using DBWTools software which uses Rietveld refinement technique. DBWS Tools for Windows 95/98/NT is a graphical interface for DBWS, one of the most used programs for Rietveld refinements. DBWS Tools handles refinement jobs by compiling Input Control Files (ICF) for DBWS, running the program and showing the graphical results using the shareware program DMPlot, which plots diffraction patterns.[10] The Rietveld plot of powder diffraction patterns are depicted in Fig. 2. The comparative analysis of experimental and calculated indicates a good fit, which was expected from the low level of residuals. The chemical composition of the major phase established from XRD data is nearly identical to the known composition of the material. Therefore, the

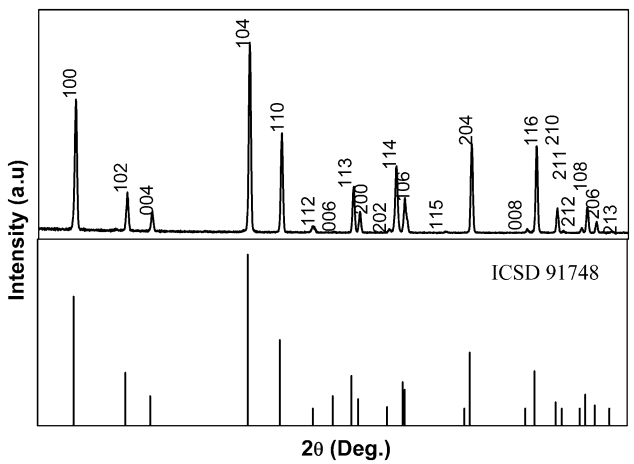

Fig. 1. Diffraction patterns of the observed data and ICSD number.

outcome of this crystal structure determination may be accepted as satisfactory. The presence of an impurity phase in this specimen was not detected, and the structure was included into a "normal" Rietveld refinement process. The figures of merit are customarily used to characterize both the full pattern decomposition and Rietveld refinement quality. The four values of the figures of merit (residual profile R_p, the expected profile residual R_{exp}, the weighted residual profile R_{wp} , and the goodness of fit χ^2) and the lattice parameters with angles are shown in Table I.

Dielectric Properties

The relation of frequency to dielectric constant (ε_{Re}) at different temperatures for both MN00 (a) and MN02 (b) is depicted in Fig. 3. A relaxation is observed in the entire temperature range as a gradual decrease in ε_{Re} as increasing frequency.

The nature of dielectric permittivity related to free dipoles oscillating in an alternating field may be described in the following way. At very low frequencies ($f \ll 1/2\pi\tau$) τ is the relaxation time), dipoles follow the field and $\varepsilon_{Re} \approx \varepsilon_S$ (value of the dielectric constant at quasi-static field). As the frequency increases ($f < 1/2\pi\tau$), dipoles begin to lag behind the field and ε_{Re} slightly decreases. When frequency reaches the characteristic frequency ($f = 1/2\pi\tau$) the dielectric constant drops (relaxation process). At very high frequencies ($f \gg 1/2\pi\tau$), dipoles can no longer follow the field and $\varepsilon_{Re} \approx \varepsilon_\infty$ (high-frequency value of ε_{Re}).[11,12] Qualitatively, this is the behavior observed in Fig. 3 for both MN00 (a) and MN02 (b) samples. It is observed that at temperatures above 380°C, the permittivity exhibits a significant increment of values. It is evident that the dielectric constant decreases as increasing frequency. In the starting low frequency range ε has higher values.[13] The ε values decreased gradually as the frequency increased from 10 Hz to 10 kHz and then decreased slowly and become almost constant up to 1 MHz for all specimens.[14,15] The observations may be explained by the phenomenon of dipole relaxation. This is due to the inability of the electric dipoles to switch with the frequency of the applied electric field.[16] The low-frequency dielectric dispersion increased with increase in V_2O_5 addition.

Complex Impedance Analysis

Complex impedance spectroscopy analysis (CISA)[17] is a powerful technique for the characterization of electrical behavior of ceramic materials,

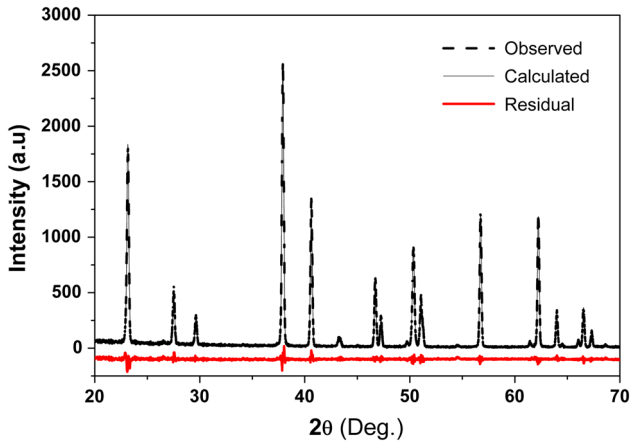

Fig. 2. The observed and calculated powder diffraction patterns of $Mg_4Nb_2O_9$ after Rietveld refinement.

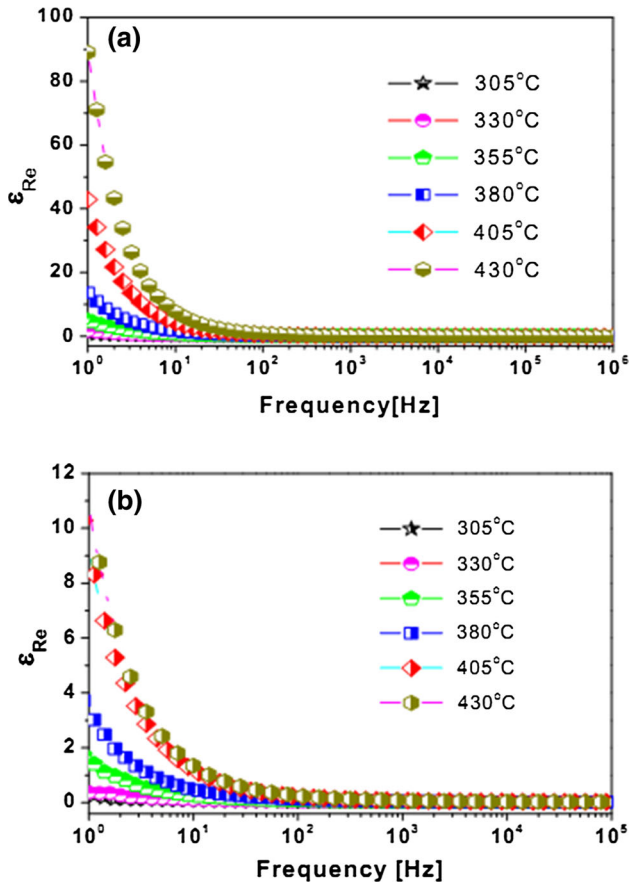

Fig. 3. Real parts of permittivity as a function of frequency at different temperatures for MN00 and MN02.

Table I. The refinement residues of Rietveld method and lattice parameters

R_p	R_{exp}	R_{wp}	χ^2	a (Å)	b (Å)	c (Å)	α (°)	β (°)	γ (°)
7.39%	11.30%	12.03%	1.06	5.1609	5.1609	14.020	90	90	120

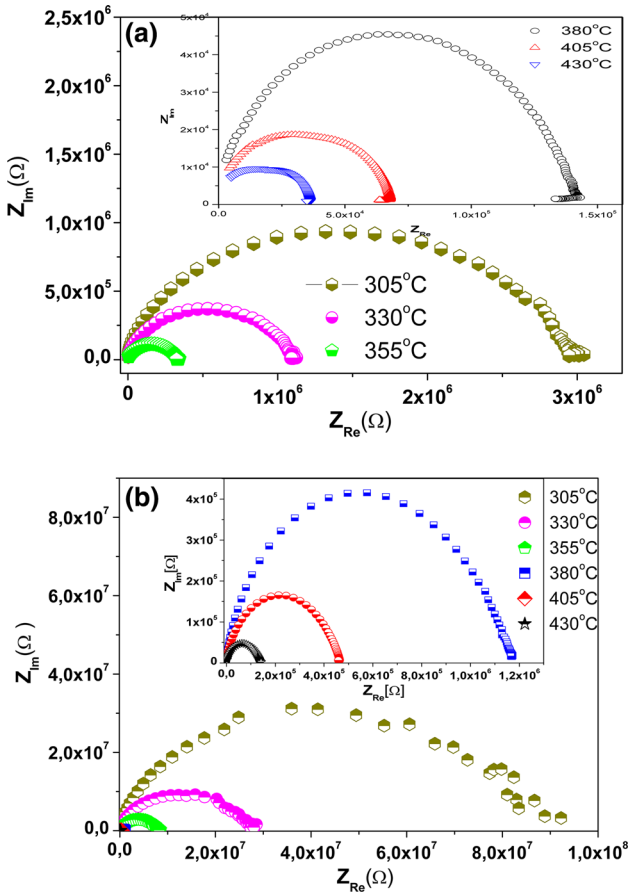

Fig. 4. The complex impedance plane plots for the MN00 (a) and MN02 (b) specimens at different temperatures. The inset shows an expanded view of the high temperatures.

where a sinusoidal wave is applied and the ac response is analyzed. In this present paper, the impedance is measured as a function of frequency at different temperatures. The results can be seen in the form of a succession of semicircle arcs representing electrical phenomena due to bulk, grain boundary effect, and interfacial phenomena in the Argand plane.[18] The frequency-dependent electrical properties of a material are represented in terms of complex impedance Z^*, as follows,

$$Z^* = Z_{\mathrm{Re}} - \sqrt{-1}Z_{\mathrm{im}}, \tag{1}$$

where Z_{Re} and Z_{Im} are the real and imaginary components of impedance, respectively; $j = \sqrt{-1}$ is the imaginary factor. Real parts of impedance with imaginary parts of impedance provide important details about the conducting behavior of the materials. The imaginary and real parts of complex impedance were plotted by using experimental data taken over a particular frequency range (1 Hz–1 MHz) at different temperatures (305–430°C) as a Nyquist diagram or complex impedance spectra of the pure specimen MN00 and the V_2O_5 added specimen MN02. For the quantitative analysis of the impedance spectrum for this present work was adopted the Cole–Cole formalism by using the equation as follows:

$$Z^* = Z_\infty + \frac{(Z_S - Z_\infty)}{1 + (\sqrt{-1}2\pi\tau)} \tag{2}$$

Here, Z_∞ and Z_s are the high and low frequency limit of the impedance, respectively, and $Z_s - Z_\infty$ is resistance strength, τ is the mean relaxation time

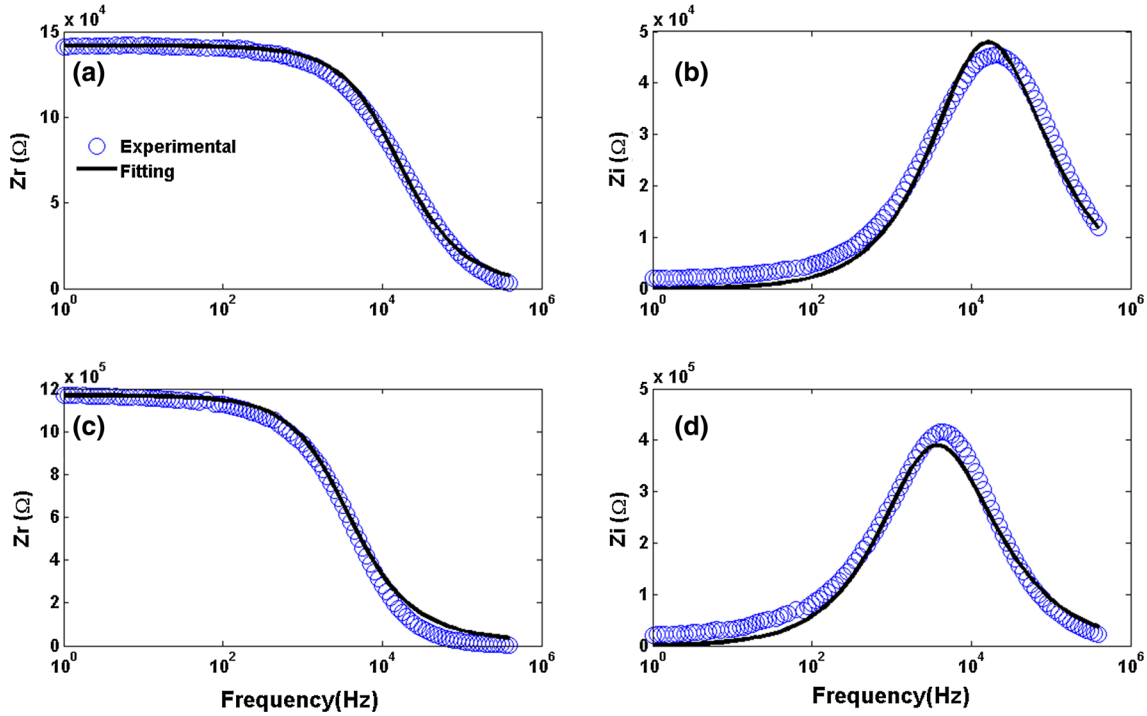

Fig. 5. Real and imaginary parts of complex impedance fitted by Cole–Cole function for MN00 (a, b) and MN02 (c, d) at 380°C.

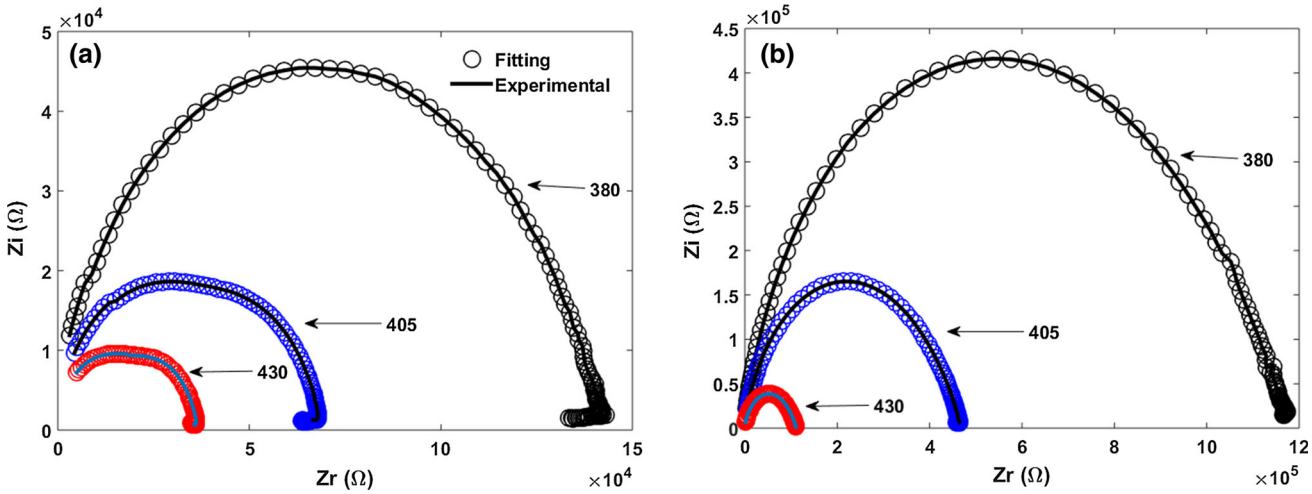

Fig. 6. Nyquist semicircle curves fitted by Cole–Cole formalism for MN00 (a) and MN02 (b) at 380°C, 405°C, and 450°C, respectively.

Table II. Simulation parameter for Cole–Cole fitting function

Sample	Temperature (°C)	α	τ	Z_S	Z_∞
MN00	380	0.7673	8.06×10^{-5}	2.972×10^{6}	1810
MN00	405	0.7676	3.06×10^{-5}	1.093×10^{6}	2907
MN02	380	0.7680	24.00×10^{-4}	9.083×10^{7}	863
MN02	405	0.7272	8.04×10^{-4}	2.877×10^{7}	1440

and α represents the distribution of relaxation time. It is also observed for both MN00 and MN02 specimens that at high temperatures the arcs decrease their magnitudes and their curves shift towards real (Z_{Re}) axis in Fig. 4. The semicircular arcs are representative of a grain effect, which in the long run, on electric conductivity may originate from a grain boundary potential barrier. From the intercepts of the each semicircular arc with the real axis, the resistance of the grain and the resistance of the grain boundary can be obtained.[19] Therefore, the complex impedance plot of both specimens (MN00 and MN02) exhibited one impedance arc and obey the Cole–Cole-type relaxation. Then, the one semicircular arc is representative of the bulk properties of the grain. In addition, according to the semicircular arcs of the MN02 specimen there is an intensity decrease of them comparing to MN00 specimen probably due to the addition of V_2O_5. Obviously, there is only a single semicircle present in both specimens and this semicircle should be corresponding to the $Mg_4Nb_2O_9$ specimen and in principle it can be fitted with a single R–C circuit. All the samples reveal dispersion due to Maxwell–Wagner[20,21] type interfacial polarization in agreement with Koop's phenomenological theory.[22,23] The high value of dielectric constant observed at lower frequencies can be explained on the basis of space charge polarization due to inhomogenities in structure like impurities, porosity and grain structure.[24]

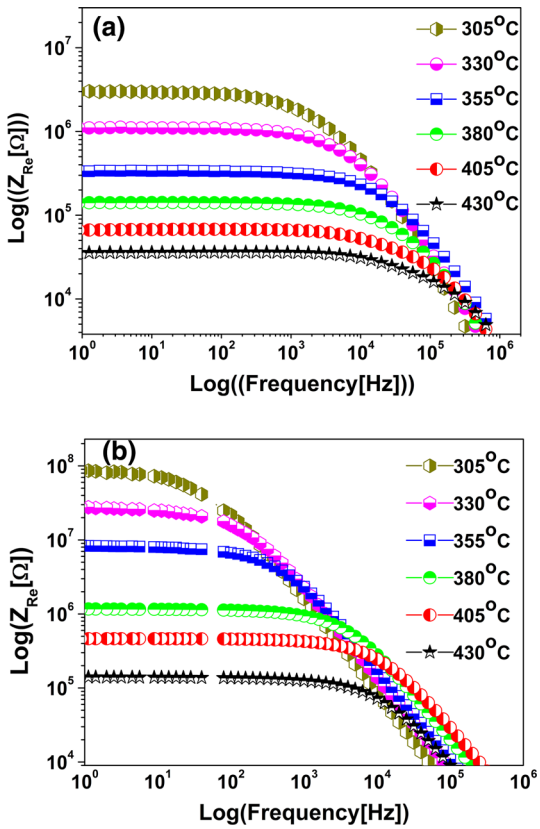

Fig. 7. Frequency dependence of Z_{Re} for MN00 (a) and MN02 (b) specimens at different temperature.

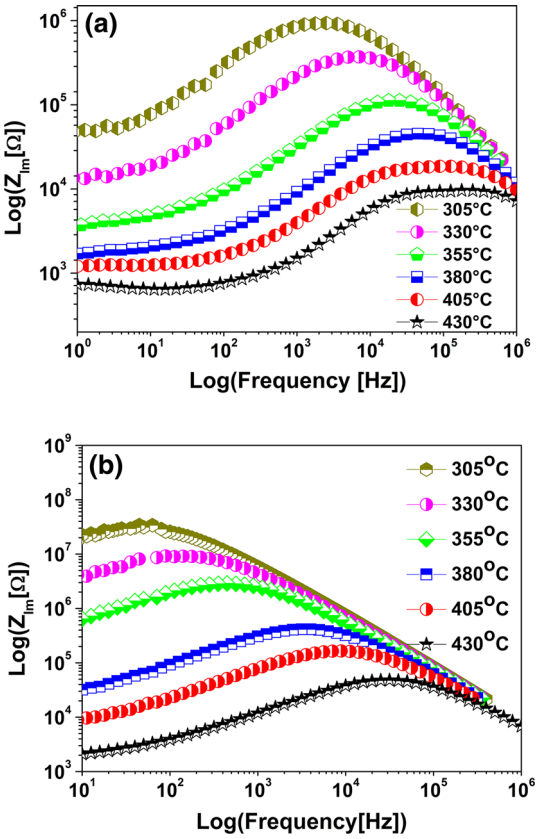

Fig. 8. Frequency dependence of Z_{Im} of MN00 (a) and MN02 (b) specimens at different temperatures.

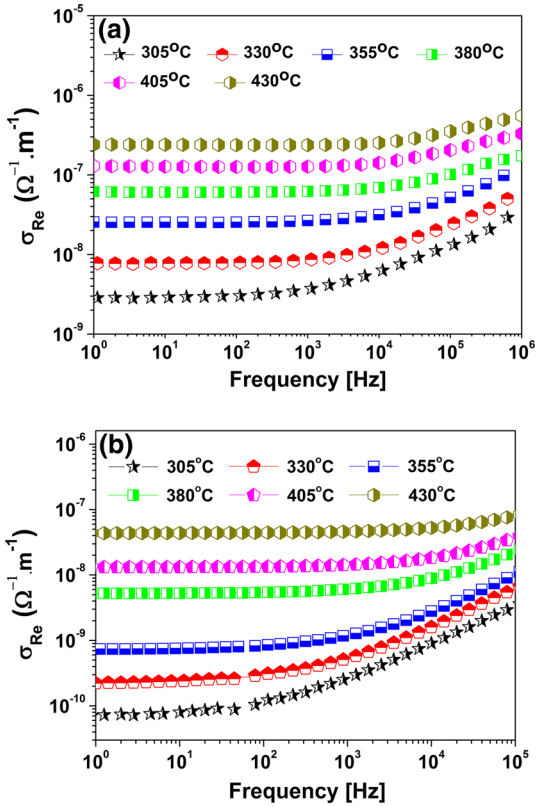

Fig. 9. Frequency dependence of ac conductivity at different temperatures for (a) MN00 and (b) MN02.

Moreover, the resistance of the material, which is determined by the semicircle diameter, decreases as increasing temperature, this behavior indicates that the temperature coefficient will be negative.[25]

In order to confirm that the Cole–Cole relaxation model is appropriate to represent the experimental data, both MN00 and MN02 specimens were fitted by using Eq. 3 with the help of a computer program elaborated to give adequate experimental data to Cole–Cole formalism showing a good fit for the experimental data at 405°C, as shown in Fig. 5. The solid lines and open circles represent the fitting function and the experimental data, respectively, at 405°C for MN02 (top) and MN00 (bottom). The curves represent the Bode plots, which consists of Z_{Re} and Z_{Im} as a function of frequency.

Experimental data of Z_{Im} and Z_{Re} were also fitted with Cole–Cole fitting function, as shown in Fig. 6 at 405°C for MN02 and MN00 specimens, respectively. A good fit was observed, especially for higher temperatures due to less interference from lower frequency regions.

The simulation parameters for the Cole–Cole fitting function are shown in Table II, where the dispersion term α belongs to the interval $0 < \alpha < 1$ to satisfy Cole–Cole formalism, and when α is equal to 1 it expresses the Debye relaxation model. The α parameter plays a role of enlarging the curves as it increases and narrowing as it decreases. The parameter τ represents the time relaxation and it makes the curve shift to lower frequencies as increasing and to higher frequencies as decreasing. Z_s and Z_∞ are the impedances for higher and lower frequencies, respectively.

The real parts (Z_{Re}) of the complex impedance (Z^*) as a function of frequency at different temperatures for MN00 and MN02 specimens are depicted in Fig. 7. It is clearly observed with the help of log–log curves that the magnitude of Z_{Re}, hereby representing the electric resistance, decreases with increasing frequency and temperature, which for both MN00 and MN02 specimens indicates a certain reduction of grains, grain boundaries, and electrode interface resistances.[24] This phenomenon implies the negative temperature coefficient of resistance in $Mg_4Nb_2O_9$. At higher frequencies, the magnitude of Z_{Re} values for all temperatures present a limit, i.e., the Z_{Re} curves shift to the same point, suggesting a probable release of space charge and a consequent lowering of the energy barrier properties for both specimens.[25] By comparing MN02 to MN00 specimens with each other, it was observed that MN00 has a shorter dc plateau, which indicates that the direct conduction process was somehow limited by the presence of V_2O_5 addition. Consequently, at lower temperatures, the behavior of shifting toward the same point occurs earlier compared to the MN00

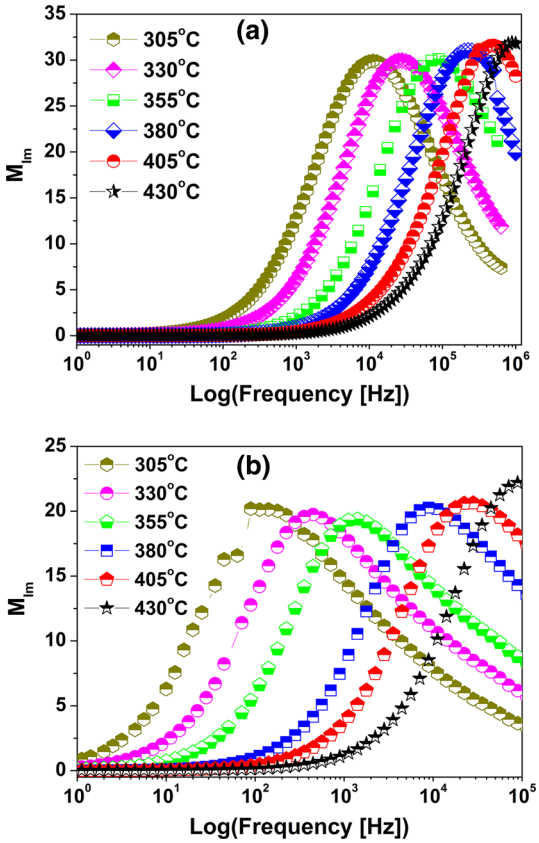

Fig. 10. Frequency dependence of the imaginary part of the electric modulus at different temperatures for (a) MN00 and (b) MN02 specimens.

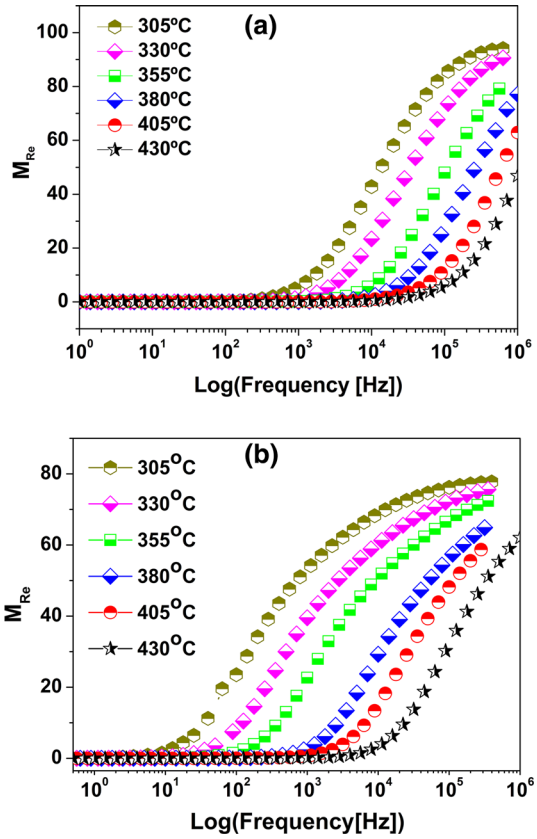

Fig. 11. Frequency dependence of the real part of the electrical modules at different temperatures for (a) MN00 and (b) MN02 specimens.

specimen. A considerable increase in magnitude of Z_{Re} for the MN02 specimen was also observed.

Imaginary parts of complex impedance (Z_{Im}) at different temperatures for both MN00 and MN02 specimens are represented by curves where the position of the relaxation peak in Z_{Im} shifts to higher frequencies with increasing temperature and an intense dispersion of Z_{Im} is observed as shown in Fig. 8b. The asymmetric broadening of the peaks, very evident for MN02 specimen, suggests the presence of electrical process of the material with a distribution of relaxation times, non-Debye model. The relaxation species may be possibly due to presence of electron at low temperature and defects at higher temperature.

It is observed that one peak appears for all temperatures, indicating the presence of only one dielectric relaxation process for both specimens. The position of the peak shifts to higher frequency with increasing temperature for both specimens. The magnitude of the peak for the MN00 specimen at different temperatures is smaller than found in MN02, probably due to the effect of V_2O_5 addition on $Mg_4Nb_2O_9$. It can be clearly seen that the first peaks at different temperatures for specimen MN02 show a typical peak broadening, whereas the peaks for specimen MN00 the broadening phenomenon presents less strong. The decrease in magnitude of peaks for both specimens as increasing temperature occurs in conformity. The frequency dependence of conductivity (σ_{AC}) at different temperatures is shown in Fig. 9 for (a) MN00 and (b) MN02 samples. The conductivity spectrum can be visually defined for two distinct regions, namely, the low-temperature region where continuous dispersion curves of conductivity are observed for both undoped and doped specimens. Then the conductivity patterns approach close to each other in the high-frequency region for the same temperature region. This may be attributed to the space charge dependent region.

The plateau region corresponds to the frequency-independent dc conductivity (σ_{DC}). The rise in the conductivity value with temperature indicates that the electrical conduction is a thermally activated process for both samples. It was also observed that the plateau is shorter for the MN02 sample than that observed for the MN00 specimen, probably because of V_2O_5 addition. The decrease of the magnitude of conductivity of the MN02 specimen compared to the MN00 sample is probably also due to the presence of V_2O_5 addition.

Using the values of electrical conductivity and modulus at 1 Hz, it was possible to relate the values of temperature and conductivity, which was

observed through the use of the Arrhenius relationship as follows, $\sigma = \sigma_0 \exp[-E_a/kT]$ for the conductivity, where σ_0 is an initial exponential factor, E_a is the activation energy of conduction process related, k is the Boltzmann constant and T is the absolute temperature in Kelvin. Variation in temperature is shown for both the pure sample as shown of MN00 and MN02 in Fig. 9a and b, respectively. In summary, the curves corresponding to the activation energy can be analyzed in the following: How do we know from the previous curves that increasing the temperature will cause a decrease in the relaxation time due to an improvement of the mobility of charge carriers in higher temperatures? This is well described by the Arrhenius-type behavior. The Arrhenius equation is used to calculate the activation energy through the value of the slope of the straight line sketch of relaxation time, where we have the maximum frequency in the imaginary part of the spectrum of the modulus.

The electrical response of the system can also be studied through complex electric modulus, which is calculated using the relation:

$$M^* = 1/\varepsilon^* = M_{Re} + jM_{Im} \quad (3)$$

Note that electric module (M^*) scales inversely to the complex permittivity, that is the more conductivity loss contributes to the permittivity, the less conductivity loss affects the electric modulus.

The imaginary parts of complex electrical modulus of the MN00 (a) and MN02 (b) samples are shown in Fig. 10. It is observed that the peaks are frequency and temperature dependent, which is clearly confirmed for the pure specimen MN00 where the peaks appear more shifted to the right with increasing temperature. It was also observed that the MN00 specimen has nearly the same peak magnitudes, and at lower temperature there is a more displaced peak to the left. In relation to MN02 specimen, it can be seen that the six curves at 305°C, 330°C, and 355°C are slightly shifted to the right, which differs from the three curves at 380°C, 405°C, and 430°C that are more shifted to the left, as shown in Fig. 10. The variation of M_{Re} increases with increasing frequency and reaches constant value, M_∞ [$M_{Re}(\omega)$ asymptotic value for high frequencies]. In Fig. 10a the domains of this transition, peaks in the values of M_{Im}, are formed providing a relaxation process. A peak position shifts to the high frequencies as increasing temperature. Consequently, this means that a relaxation stops this convection process as increasing temperature.

The variation of real part of electric modulus M_{Re} as a function of frequency over a range of temperature is given in Fig. 11a. The value of M_{Re} is very low (approaching zero) in the low frequency region. As frequency increases the value of M_{Re} increases and reaches a maximum constant value of $M_\infty = 1/\varepsilon_\infty$ at higher frequencies for all temperatures.[26]

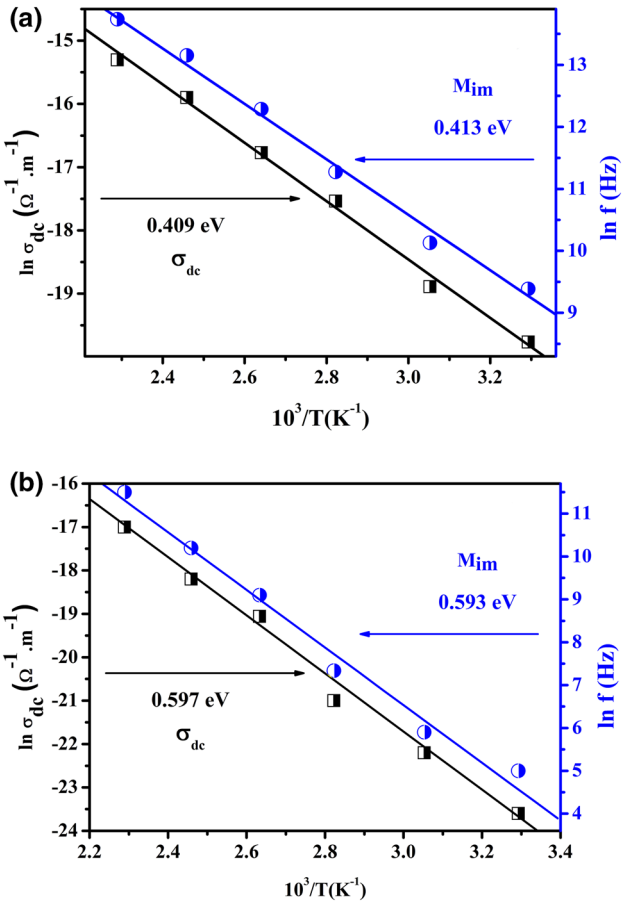

Fig. 12. Shows activation energy for (a) MN00 (b) MN02 samples.

Figure 12 shows the values of the activation energy for the conductivity of approximately 0.409 eV, which is close to the modulus 0.413 eV values, indicating that the electrical entities involved and responsible for the electrical conduction and the relaxation process observed in M^* are the same. The activation energies of 0.597 eV and 0.593 eV related to the MN02 specimen were found for conductivity and the modulus, respectively. Hereby, comparing with the pure sample, an increase in activation energy is probably due to the addition of V_2O_5. Thus, we use both direct conductivity and the imaginary part of modulus for plotting the charts of the activation energy initially for MN00 MN02 specimens. The MN05 specimen presents an activation energy of 0.68 and 0.78 eV calculated by conductivity and the complex modulus, which are two values less close comparing to the MN00 and MN02 specimens. Finally, we have the MN10 sample, which obtained a 0.58 eV activation energy determined by the conductivity and 0.46 eV calculated by the frequency to the maximum value of the modulus of complex impedance. We note that the samples MN00 and MN02 have an activation energy closer to comparing with subsequent sam-

ples where we assumed that the addition of V_2O_5 caused changes in activation energy. The curves are very close to the simulation of the experimental points both for those originating from the conductivity and the electric complex modulus. The excess of addition can affect the properties and it will always be a case of a tradeoff between the parameters to determine which best suited.

CONCLUSION

The present work reports the results of our investigation on the dielectric and electric properties of $Mg_4Nb_2O_9$ ceramic with the addition of 2% of V_2O_5 for the improvement of electrical and dielectric properties for coming microwave and radio frequencies applications. The samples were analyzed over a range of frequency (1 Hz to 1 MHz) at different temperatures (305–430°C). The dielectric constant gradually decreases with increasing frequency for all samples. Increasing the temperature, increases the dielectric constant obviously, which becomes even more significant at low frequency (below 10 Hz). Nyquist diagrams which is represented by semicircular arcs have indicated a single relaxation phenomenon for both MN00 and MN02 specimens. Modulus analysis indicates non-exponential type conductivity relaxation in the material and the activation energy calculated from electric modulus and conductivity for both MN00 and MN02 specimens are ~0.409 eV (σ_{DC})/~0.413 eV (M_{Im}) and ~0.597 eV (σ_{DC})/~0.593 eV (M_{Im}), respectively.

ACKNOWLEDGEMENTS

The authors are grateful to CAPES, LOCEM Laboratory, x-ray Laboratory, and the US Air Force Office of Scientific Research (AFOSR) (FA9550-16-1-0127).

REFERENCES

1. J.D. Guo, C.Y. Li, Q.J. Mei, G. Wang, H.T. Wu, and Q. Zou, *Mater. Technol.* 30, 3 (2015).
2. M.H. Sarrafi, H.B. Bafrooei, M. Feizpour, T. Ebadzadeh, and M.H. Foroush, *J. Mater. Sci. Mater. Electron.* (2016). doi:10.1007/s10854-013-1668-2.
3. R. Cao, C. Cao, X. Yu, and J. Qiu, *Luminescence* (2014). doi: 10.1002/bio.2711.
4. T.-H. Fang, Y.-J. Hsiao, L.-W. Ji, Y.-S. Chang, and S.-S. Chi, *J. Cryst. Growth* 310, 3331 (2008).
5. G.G. Yao, C.J. Pei, H. Ma, H.L. Zhang, and X.L. Tian, *J. Ceram Process. Res.* 13, 93 (2012).
6. Y.-C. Liou and Y.-L. Sung, *Ceram. Int.* 34, 371 (2008).
7. S. Ananta, *Mater. Lett.* 58, 2530 (2004).
8. H.T. Wu, Y.S. Jiang, W.B. Wu, F. Yang, and Y.L. Yue, *J. Electroceram.* (2012). doi:10.1007/s10832-012-9705-8.
9. H.T. Wua, L.X. Lia, Q. Zoua, Q.W. Liaoa, P.F. Ninga, and P. Zhanga, *J. Alloys Compd.* 509, 2232 (2011).
10. L. Bleicher, J.M. Sasaki, and C.O.P. Santos, *J. Appl. Crystallogr.* 33, 1189 (2000).
11. S. Sahoo, U. Dash, S.K.S. Parashar, and S.M. Ali, *J. Adv. Ceram.* (2013). doi:10.1007/s40145-013-0075-8.
12. N.K. Singh and P. Kumar, *Adv. Mater. Lett.* (2011). doi: 10.5185/amlett.2011.1215.
13. Z.S. Macedoa, A.L. Martinezb, and A.C. Hernandes, *Mater. Res. Ibero. Am. J.* (2003). doi:10.1590/S1516-14392003000400026.
14. S.S. Danewalia, G. Sharma, S. Thakur, and K. Singh, *Sci. Rep.* (2016). doi:10.1038/srep24617.
15. M. Slankamenac, T. Ivetic, M.V. Nikolic, N. Ivetic, M. Zivanov, and V.B. Pavlovic, *J. Electron. Mater.* (2010). doi: 10.1007/S11664-010-1118-3.
16. D.H. Wang, W.C. Goh, M. Ning, and C.K. Ong, *Appl. Phys. Lett.* 88, 496 (2011).
17. P.S. Das, P.K. Chakraborty, B. Behera, N.K. Mohanty, and R.N.P. Choudhary, *J. Adv. Ceram.* (2014). doi: 10.1007/s40145-014-0087-zCN10-1154/TQ.
18. Y.-H. Lin, M. Li, C.-W. Nan, and J. Li, *Appl. Phys. Lett.* 89, 032907 (2006).
19. J.C. Maxwell, *Electricity and Magnetism*, vol. 1 (Oxford, 1892), p. 197.
20. K.W. Wagner, *Ann. Phys.* 40, 818 (1993).
21. C.G. Koops, *Phys. Rev.* 83, 121 (1951).
22. S. Upadhyay, D. Kumar, and O.M. Prakash, *Bull. Mater. Sci.* 19, 513 (1996).
23. P.A. Jahdhav, M.B. Shelar, and B.K. Chougule, *J. Alloys Compd.* 479, 385 (2009).
24. B. Ghosh, A. Dutta, and T.P. Sinha, *J. Alloys Compd.* (2013). doi:10.1016/j.jallcom.2012.11.027.
25. M.M. Costa, G.F.M. Pires Jr, A.J. Terezo, M.P.F. Graça, and A.S.B. Sombra, *J. Appl. Phys.* 110, 034107 (2011).
26. M. Ram and S. Chakrabarti, *J. Alloys Compd.* (2008). doi: 10.1016/j.jallcom.2007.08.001.